IOP Publishing Nanotechnology
Nanotechnology 26 (2015) 164003 (9pp) doi:10.1088/0957-4484/26/16/164003

# Pd nanoparticles on ZnO-passivated porous carbon by atomic layer deposition: an effective electrochemical catalyst for Li-$O_2$ battery

**Xiangyi Luo[1,2,6], Mar Piernavieja-Hermida[3,6], Jun Lu[1], Tianpin Wu[4], Jianguo Wen[5], Yang Ren[4], Dean Miller[5], Zhigang Zak Fang[2], Yu Lei[3] and Khalil Amine[1]**

[1] Chemical Sciences and Engineering Division, Argonne National Labaratory, Argonne, IL 60439, USA
[2] Metallurgical Engineering Department, University of Utah, Salt Lake City, UT 84112, USA
[3] Department of Chemical and Materials Engineering, University of Alabama in Huntsville, AL 35899, USA
[4] X-ray Science Division, Advanced Photon Source, Argonne National Labaratory, Argonne, IL 60439, USA
[5] Electron Microscopy Center, Argonne National Laboratory, Argonne, IL 60439, USA

E-mail: junlu@anl.gov, zak.fang@utah.edu, yu.lei@uah.edu and amine@anl.gov

Received 2 December 2014, revised 19 February 2015
Accepted for publication 1 March 2015
Published 1 April 2015

**Abstract**

Uniformly dispersed Pd nanoparticles on ZnO-passivated porous carbon were synthesized via an atomic layer deposition (ALD) technique, which was tested as a cathode material in a rechargeable Li-$O_2$ battery, showing a highly active catalytic effect toward the electrochemical reactions—in particular, the oxygen evolution reaction. Transmission electron microscopy (TEM) showed discrete crystalline nanoparticles decorating the surface of the ZnO-passivated porous carbon support in which the size could be controlled in the range of 3–6 nm, depending on the number of Pd ALD cycles performed. X-ray absorption spectroscopy (XAS) at the Pd K-edge revealed that the carbon-supported Pd existed in a mixed phase of metallic palladium and palladium oxide. The ZnO-passivated layer effectively blocks the defect sites on the carbon surface, minimizing the electrolyte decomposition. Our results suggest that ALD is a promising technique for tailoring the surface composition and structure of nanoporous supports for Li-$O_2$ batteries.

Keywords: Li-$O_2$ battery, atomic layer deposition, $Li_2O_2$

(Some figures may appear in colour only in the online journal)

## 1. Introduction

The lithium-oxygen battery has received significant interest because of its extremely high theoretical energy density, which exceeds that of any other existing energy storage systems [1–22]. The cathode in the Li-$O_2$ battery consists of a porous matrix in which the discharge solid products are generated from the reaction of Li cations with $O_2$. The cathode of a Li-$O_2$ cell requires a catalyst to promote the discharge reaction. It has been found that a diversity of factors dictate the nature of electrochemical reactions in Li-$O_2$ cells, such as the nature, morphology and surface area of the catalysts, as well as the type of organic electrolyte being used [6, 16, 17, 23–26].

One of the main challenges faced by the development of Li-$O_2$ batteries is the high overpotentials on discharge and in particular on charge (>1.0 V). These high overpotentials are a

[6] These authors contributed equally.

 

consequence of the necessity of a rechargeable Li-$O_2$ battery. A large overpotential during charge, even at very low current densities, results in very low round-trip efficiencies (<60%), low power capability and poor cycle life. In order to lower the charge overpotential in the Li-$O_2$ cells, different electrocatalysts have been examined such as metals and metal oxides [1, 2, 14–17, 19, 27–31]. However, some of the early work was based on carbonate electrolytes, which have been found unstable against the superoxide anion, leading to the decomposition of the electrolytes during the discharge and charge of the cell.

The design of next-generation cathode materials for Li-$O_2$ batteries is expected to be complicated in that the batteries' capacity, discharge/charge potentials and cycle life can be affected by many factors [32]. The slow electron transport to the $Li_2O_2$/electrolyte interface due to the poor electronic conductivity of the $Li_2O_2$ discharge product may severely limit the charge process [21–23]. A higher charge potential could also result from the electrolyte decomposition, which leads to the possible formation of $Li_2CO_3$, thereby contaminating the $Li_2O_2$ discharge product. One of the major sources responsible for the electrolyte decomposition, especially in the ether-based electrolytes, may result from reaction of the electrolyte with defects on the carbon surface, which can occur at voltages as low as 3.5 V during a charge in the presence of $Li_2O_2$. However, based on the theoretical calculation, the charge overpotential for a $Li_2O_2$ film is only ~0.2 V, assuming that the electron transport to the $Li_2O_2$/electrolyte interface has no limitations [26]. Therefore, the charge overpotential of the Li-$O_2$ cell could be significantly reduced if the aforementioned issues can be addressed.

To understand the intrinsic properties of the cathode materials, it is also necessary to reduce the number of variables to a tractable level. ALD, which is a technique that enables conformal coatings of thin films and nanoparticles on both planar and porous substrates [33–35], allows one to obtain a well-defined cathode architecture. It employs the surface self-limiting reactions between organometallic precursors and the targeted substrate, allowing atomic precision control over the composition and thickness of the thin film as well as the diameter of the nanoparticles. The composition and thickness of the coating materials can be precisely tuned by mixing the proper order, number and ratio of the ALD processes. In addition, by taking advantage of the difference in surface reaction rate, i.e. the surface reaction on one type of surface is significant faster than the other, one can selectively deposit the coating materials onto the targeted surface [36–38]. This characteristic is attractive for the synthesis of nanostructured architecture, e.g., core–shell nanoparticles and tandem bilayer nanostructure.

In this paper we describe an approach based on a cathode architecture that has a protective ZnO coating passivation layer on a porous carbon substrate. ALD was applied to prepare these cathode architectures, which addresses the electrolyte decomposition problem by passivating the surface defect sites on the porous carbon. As a consequence, the air cathode based on this modified architecture shows promising results for solving the charge overpotential problem. Bulk zinc oxide (ZnO) has a direct band gap of 3.3 eV, much smaller compared to that of bulk $Al_2O_3$ (8.8 eV). ZnO ALD using alternating exposures to diethylzinc and water is well understood and provides conformal coatings [39]. In addition, the growth rate of Pd is faster on the ZnO surface than the $Al_2O_3$ surface [40]. All the above advantages make ZnO a promising material as the passivating layer on carbon. Here, we demonstrated that a cathode architecture with uniformly dispersed palladium nanoparticles onto a ZnO-passivated porous carbon substrate prepared by ALD shows high electrochemical catalytic activity in a Li-$O_2$ cell. This cathode architecture reduced the charge overpotential to almost 0 V, which is the lowest ever reported. The discharge products are characterized by x-ray diffraction (XRD) and scanning electron microscopy (SEM). The effect of the Pd loading on the electrochemical performance of the Li-$O_2$ cell is also investigated.

## 2. Experimental details

The Pd/ZnO/carbon cathode materials were synthesized using ALD. Pd and ZnO ALD was carried out in a commercial benchtop ALD reactor (Arradiance, Gemstar-6) equipped with an *in situ* quartz-crystal microbalance (QCM, Inficon). Ultra-High purity nitrogen carrier gas (Airgas, 99.999%) was further purified using a Supelco gas purifier (Sigma-Aldrich) to trap hydrocarbon, moisture and oxygen-containing impurities before entering the reactor.

Graphitized carbon black (Sigma-Aldrich) with an average particle size of 330 nm and a surface area of 70 $m^2\ g^{-1}$ was used as the substrate without further treatment. Graphitized carbon black was uniformly spread onto a stainless steel sample tray with a stainless steel mesh top to contain the powder while still supplying access to the ALD precursor vapors. The loaded sample tray was placed into the center of the reactor and kept for at least 30 min at 200 °C in a 50 sccm flow at 0.5 Torr pressure to allow temperature stabilization and to outgas the carbon.

The ZnO ALD used alternating exposures to diethylzinc (DEZ, Sigma-Aldrich, Zn 52.0 wt%) and deionized water at 200 °C. The Pd ALD used alternating exposures to Pd(II) hexafluoroacetylacetonate ($Pd(hfac)_2$, Sigma-Aldrich, 98%) and formalin (Sigma-Aldrich, 37 wt% in $H_2O$ with methanol added for stability). All the precursor bubblers were kept at room temperature except the $Pd(hfac)_2$ bubbler, which was kept at 70 °C during the Pd ALD. The ALD timing sequences can be expressed as $t_1$-$t_2$-$t_3$-$t_4$, where $t_1$ and $t_3$ correspond to the exposures times of the two precursors, $t_2$ and $t_4$ are the nitrogen purge times between precursor exposures and all units are given in seconds. The timing sequence used for the seed layer was ZnO 0.5-60-0.75-60. The samples were prepared using 2 and 5 cycles of ZnO. For Pd ALD the time sequence utilized was 300-900-200-600. Graphitized carbon black was first passivated using 2 and 5 ALD cycles of ZnO, followed by 1, 3 and 10 ALD cycles of Pd. The samples were denoted as 1c-Pd/2c-ZnO/C, 3c-Pd/2c-ZnO/C, 10c-Pd/2c-ZnO/C and 3c-Pd/5c-ZnO/C, respectively.

The electrochemical characterization was carried out using a Swagelok-type cell composed of a lithium metal anode, a glass fiber separator impregnated with ether electrolyte (TEGDME 1 M $LiCF_3SO_3$) and a porous cathode (7/16 inch diameter). The cathode was formed by mixing the as-prepared cathode material and binder in a molar ratio of 80:20. The cells were sealed in a 1 bar pure $O_2$ atmosphere to avoid any negative effects of humidity and $CO_2$. The electrochemical measurements were carried out using a MACCOR cycler under a constant current density of 100 mA $g^{-1}$. The observed capacity was calculated based on the weight of the cathode active material in this study.

High-energy synchrotron XRD was used to characterize the discharge products. Such characterization was carried out at the 11-ID-C beamline of the Advanced Photon Source (APS), Argonne National Laboratory. The x-ray wavelength was 0.111 65 Å. The samples were completely protected with Kapton tape from any side reactions from the air. The XRD patterns were collected in the transmission mode using a Perkin Elmer large area detector. The collected two-dimensional patterns were then integrated into conventional one-dimensional patterns for final data analysis using the Fit2d software.

SEM images were taken on a Hitachi S5500 at 0.5 kV, and the TEM images were taken by a field-emission transmission electron microscope (FEI Titan 80-300ST) with a spherical and chromatic aberration imaging corrector working at 80 kV. Spherical and chromatic aberration correction enables the microscope to attain resolution better than 0.1 nm (measured by Young's fringes) at 80 kV.

Pd K-edge (23.564 keV) XAS was performed at the 9-BM beamline at the APS. The amount of the sample in use was optimized to achieve an XAS step height of about 1. The XAS spectra were recorded in transmission mode. Standard procedures based on WINXAS 3.1 software were used to fit the data in the extended x-ray absorption fine structure (EXAFS) regime. The EXAFS coordination parameters were obtained by a least-square fit in $q$- and $r$-space of the isolated nearest neighbor $k^2$- weighted Fourier transform data.

## 3. Results and discussions

The oxidation state and nearest neighbors of the palladium nanoparticles were determined using x-ray absorption near edge structure (XANES) spectra recorded in an ambient condition. The XANES spectra of 1c-, 3c- and 10c-Pd on ZnO-passivated carbon are showed in figure 1(a). Similar to our previous study [41], Pd step edges show a slight shift to lower energy and decreasing whiteline intensity with increasing ALD cycles, suggesting a decrease in the percentage of the oxide's component for the Pd nanoparticles. The XANES linear combination fit was performed to estimate the metal and oxide composition. The Pd nanoparticles primarily exist in the metallic form with 20–25% oxide species. The percentage of the PdO component decreased with increasing ALD cycles. Increasing

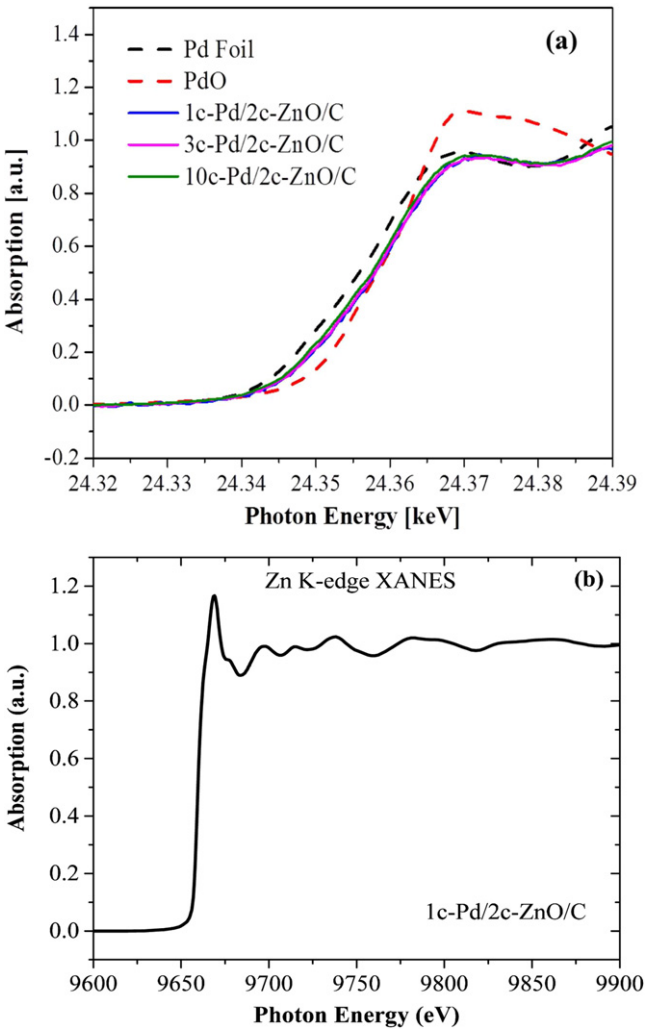


**Figure 1.** (a) Pd K-edge XANES spectra for the reference samples Pd foil and PdO and for the as-prepared Pd/ZnO/C samples, (b) Zn K-edge XANES spectra 1c-Pd/2c-ZnO/C sample.

ALD cycles lead to an increase in the Pd nanoparticle diameter as well as a decrease in the percentage of Pd surface atoms. The XANES fittings clearly suggest that the surface Pd atoms are oxidized and that the core of the nanoparticles remains metallic. The presence of ZnO on the carbon surface is also confirmed by the XANES data, shown in figure 1(b).

Figures 2(a) and (c) illustrate the representative TEM images of the 1-cycle and 3-cycle ALD-Pd on ZnO-passivated carbon samples, respectively, which demonstrate a uniform dispersion of the Pd nanoparticles over the carbon substrate. The average size of the Pd nanoparticles was determined to be around 3 nm and 6 nm for 1-cycle and 3-cycle ALD-Pd samples, respectively. Compared to the conventional metal oxide surfaces, the Pd particles prepared under similar conditions show a much larger particle size on porous carbon [42, 43]. In addition, a much higher density of Pd nanoparticles is normally achieved than that on porous carbon due to fewer nucleation sites for the Pd ALD on the carbon substrate, and that Pd diffuses more rapidly on the carbon, yielding a smaller number of larger particles.

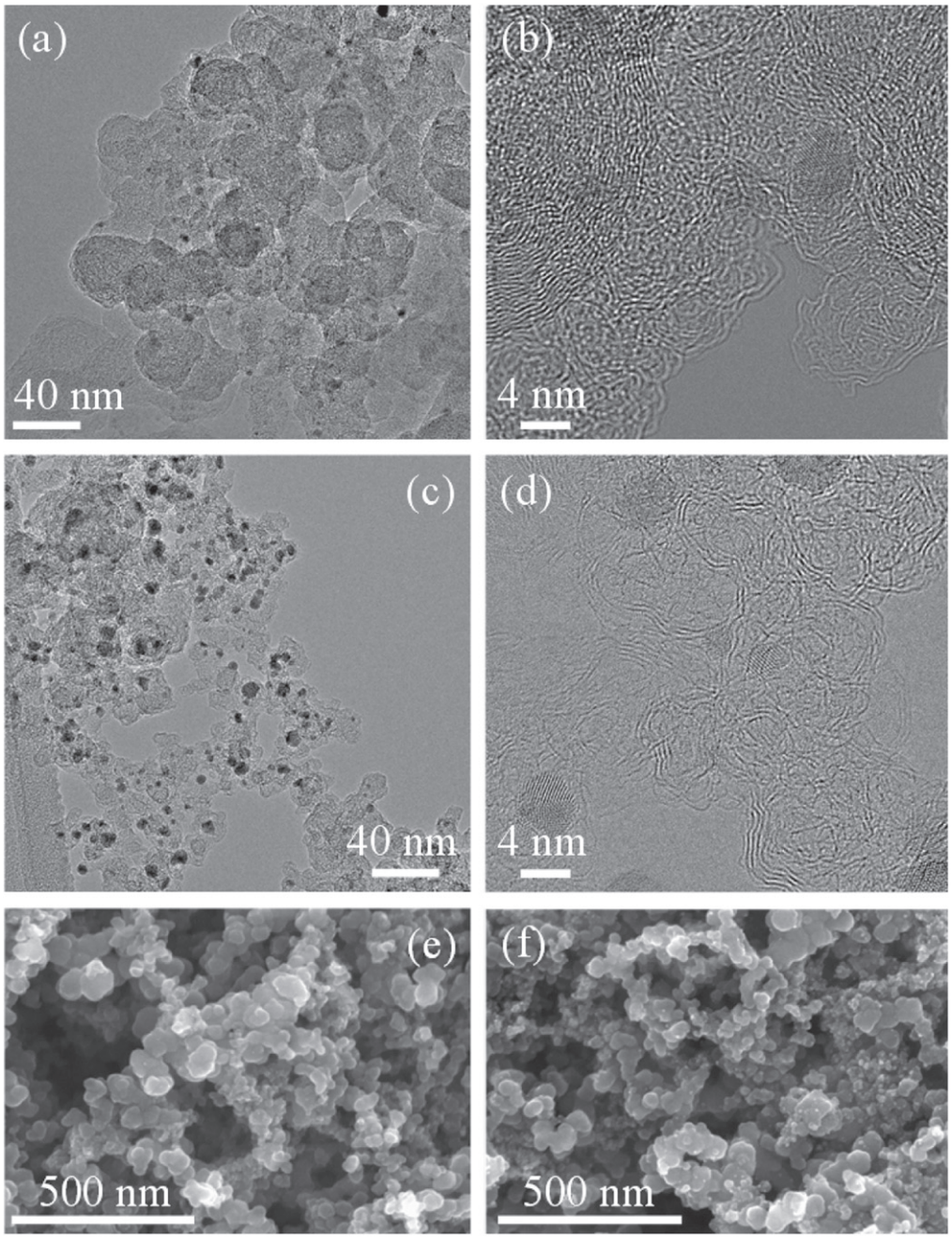


**Figure 2.** TEM images for the (a), (b) 1c-Pd/2c-ZnO/C and (c), (d) 3c-Pd/2c-ZnO/C samples. SEM images for the (e) carbon substrate and (f) 10c-Pd/2c-ZnO/C sample.

The dispersion of Pd on carbon surface is still very uniform. These TEM images clearly indicate that the diameter of the Pd nanoparticles increases along with increasing ALD cycles, which is consistent to the XANES results. Figures 2(b) and (d) show the typical high-resolution TEM images for 1-cycle and 3-cycle ALD-Pd samples, respectively. The lattice fringes for the metal nanoparticles are clearly visible for both samples, indicating that Pd nanoparticles are well crystalline and faceted. The lattice fringes of the nanoparticles are measured to be ~0.23 nm, consistent with the d-spacing for the Pd [111] plane [44]. It should also be pointed out that the porous structure of carbon is well preserved during the process of synthesizing Pd nanoparticles on ZnO-passivated carbon samples by ALD, as shown in figures 2(e) and (f). A well-preserved porous structure with the appropriate pore size is expected to show high electrochemical performance since it has been considered as one of the major factors that has significant impact on cell capacity and cycle life in Li-$O_2$ cells.

The electrochemical performance of these cathode architectures was evaluated in a Swagelok-type cell under 1 atm $O_2$ atmosphere with a MACCOR cycler. The cell consists of a Li-foil anode, an as-prepared Pd/ZnO/C cathode and a TEGDME-$LiCF_3SO_3$ electrolyte due to its greater

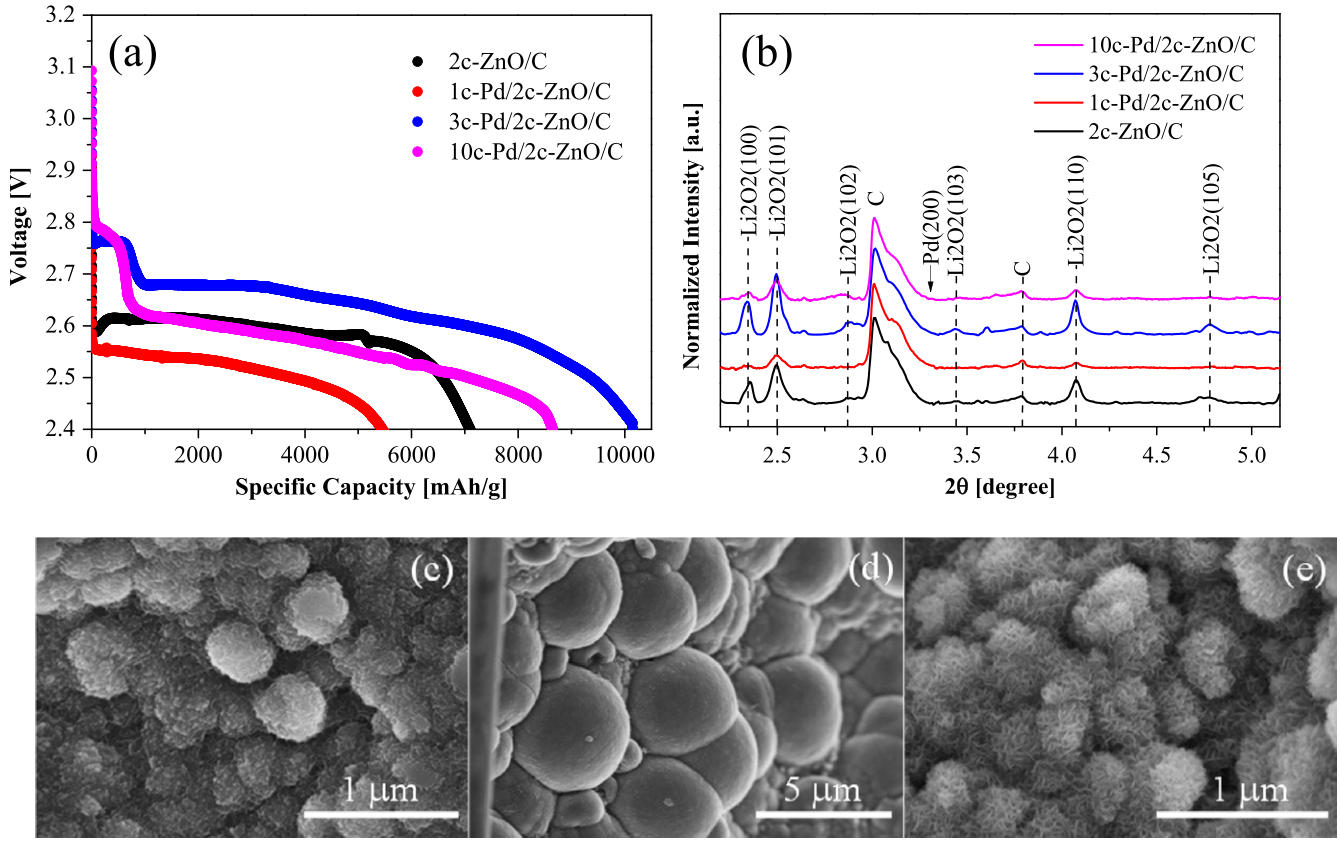


**Figure 3.** (a) Voltage profiles and (b) XRD patterns of the cathodes discharged to 2.4 V. SEM images for the discharge cathodes (c) 1c-Pd/2c-ZnO/C, (d) 3c-Pd/2c-ZnO/C and (e) 10c-Pd/2c-ZnO/C.

stability toward the discharge product. For comparison, carbon with 2 ALD cycles of ZnO without Pd nanoparticles (2c-ZnO/C) was also evaluated using the same cell configuration described above. Figure 3(a) shows the voltage profiles of the first discharge at 2.4 V under a current rate of 100 mAh $g^{-1}$ for all the samples. The initial discharge plateau for the 3c-Pd/2c-ZnO/C sample occurs at approximately 2.75 V with a capacity of 1000 mAh $g^{-1}$, which slightly drops to below 2.7 V with a total discharge specific capacity exceeding 10 000 mAh $g^{-1}$. The rest of the cells with different Pd loadings (1c-ALD and 10C-ALD samples), however, delivered much less capacity at a lower discharge plateau. It is believed that the discharge capacity of a cell is strongly dependent on the active site on the cathode surface, including that of catalyst nanoparticles. For the 1c-Pd/2c-ZnO/C sample, the loading of Pd nanoparticles is too low to provide enough active sites for the oxygen reduction reaction; the 10c-Pd/2c-ZnO/C sample provides enough Pd loading, but the active sites are reduced due to the aggregation of the Pd particles compared to the 3c-Pd/2c-ZnO/C sample. Therefore, Pd loading with the 3-cycle ALD, e.g. the 3c-Pd/2c-ZnO/C sample, has the highest active site for the oxygen reduction reaction, which leads to a higher discharge capacity. The effects of the catalyst clusters on the formation of discharge products has been reported in our previous work [45], which demonstrated dramatically different morphologies of the electrochemically grown lithium peroxide dependent on the size of the Ag clusters as the electrocatalyst. It is also interesting to note that the cell containing 2c-ZnO/C (without Pd loading) as the cathode delivered higher capacity than that of the 1c-Pd/2c-ZnO/C sample. Clearly, either the loading or the particle size of the Pd nanoparticle on the ZnO-passivated porous carbon has significant impact on the discharge capacity of the Li-$O_2$ cell.

Figure 3(b) shows the XRD patterns for cathodes harvested after first discharged, which clearly demonstrates that $Li_2O_2$ is the main discharge product for all the samples tested in this study. No evidence shows other crystalline species, such as $Li_2CO_3$ or LiOH, in the discharge products, although some amorphous compounds cannot be ruled out. Peaks corresponding to the (100), (101), (102), (105) and (110) planes can be indexed to a hexagonal structure $Li_2O_2$, which is consistent with the previous reported data. In addition, it can be observed that the intensity of $Li_2O_2$ for the 3c-Pd/2c-ZnO/C sample is much stronger than the other Pd-ZnO-C samples, mainly due to the larger discharge capacity of the former sample. The SEM images of the same discharged cathodes clearly show a large amount of toroid particles covering the whole surface of the sample, which is the typical morphology of $Li_2O_2$, as reported earlier [17] (see figures 3(c)–(e)). However, it appears that the size of the toroidal particle on the discharged 3c-Pd/2c-ZnO/C cathode is much denser and larger than those of the other samples, although a few smaller toroids are also visible

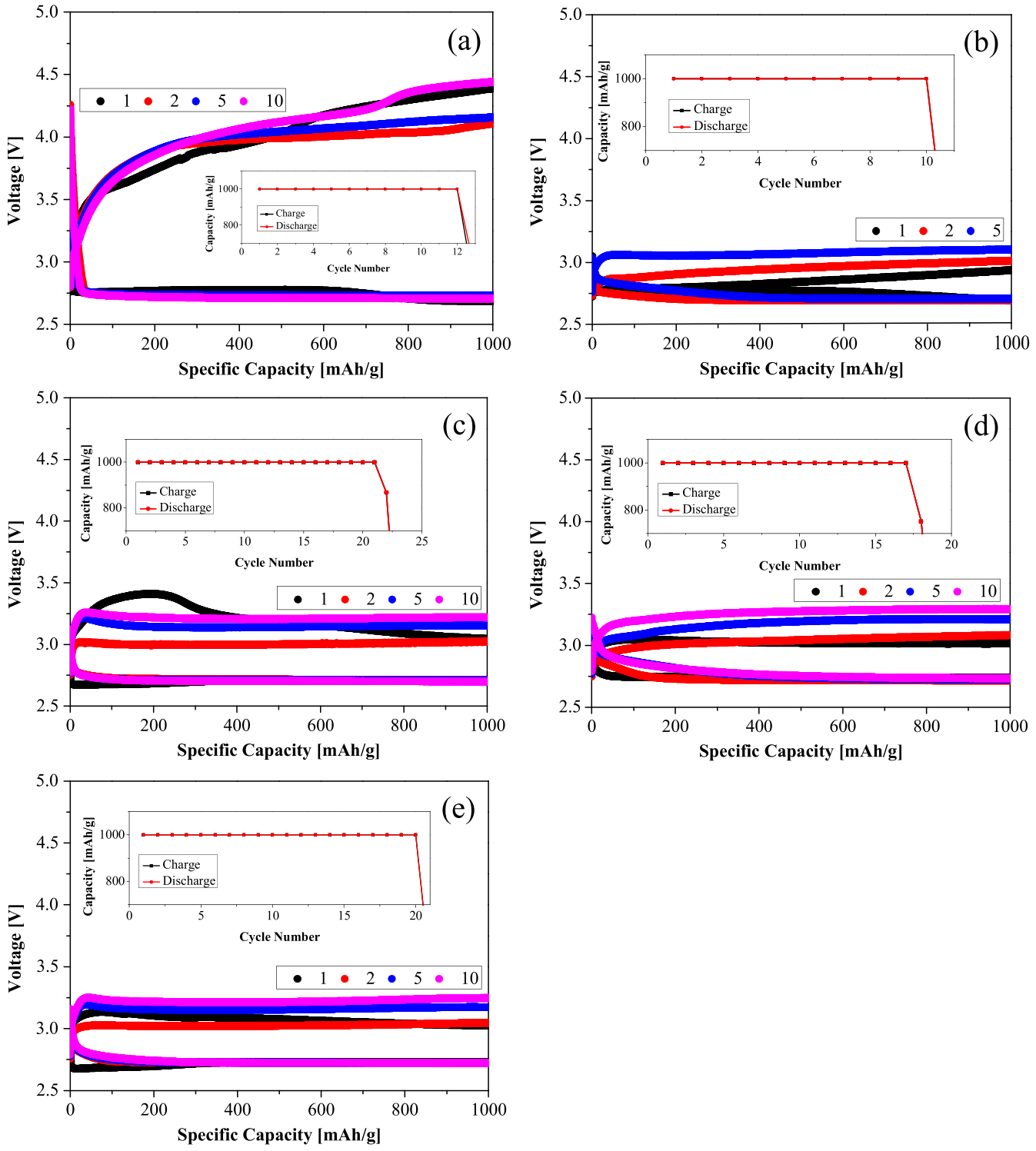


**Figure 4.** Voltage profiles recorded from the discharge/charge cycles obtained from the cells (a) 2c-ZnO/C, (b) 1c-Pd/2c-ZnO/C, (c) 3c-Pd/2c-ZnO/C, (d) 10c-Pd/2c-ZnO/C and (e) 3c-Pd/5c-ZnO/C.

between the bigger ones, as marked in the figure. Moreover, careful examination of the SEM images indicates that the building blocks of the toroidal discharge products of the Pd/ZnO/C-based cathodes are distinctly different, i.e. 10c-Pd/2c-ZnO/C discharge products are made up of nanofibers; 1c-Pd/2c-ZnO/C discharge products consist of smaller and more spherical nanoparticles, while 3c-Pd/2c-ZnO/C discharge products contain much bigger and denser nanoparticles. This finding provides strong evidence that the oxygen reduction reaction during discharge in the Li-$O_2$ cell is significantly altered when Pd nanoparticles on ZnO-passivated carbon is used as the electrocatalyst, which not only contributes to a higher capacity by providing more active sites for the ORR reaction in the case of 3c and 10c ALD-Pd samples but also leads to a different morphology of the discharge products.

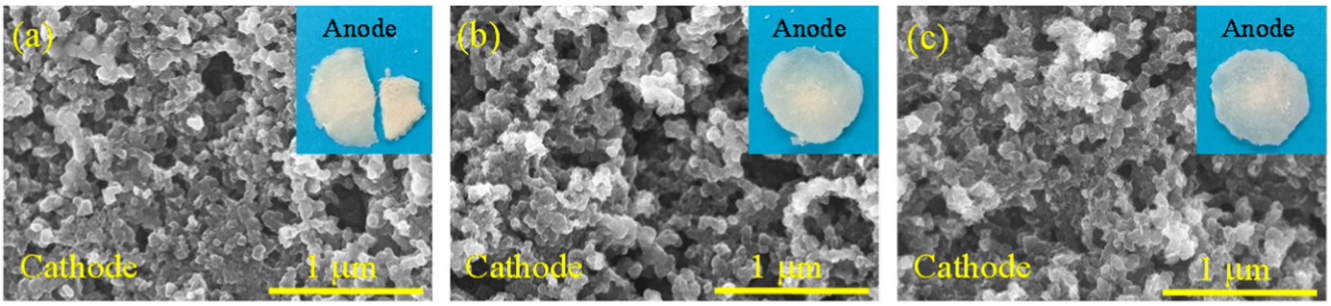


**Figure 5.** SEM images for cathodes and images of the degraded Li anode after discharge/charge cycles (stop at charge) (a) 1c-Pd/2c-ZnO/C, (b) 3c-Pd/2c-ZnO/C and (c) 10c-Pd/2c-ZnO/C.

In order to reveal the catalytic activity on the oxygen evolution reaction (charging) of the Pd/ZnO/C-based cathodes, we applied a capacity-controlled mode to investigate the discharge/charge behavior of the Li-$O_2$ cell [41, 45]. Under this mode, the cutoff charging condition is specified so that the charge capacity matches the previous discharge capacity, in this case 1000 mAh $g^{-1}$, while charge potential is limited to 4.5 V. Figure 4 shows voltage profiles recorded from the discharge/charge cycles obtained from the cells with the two different types of cathode architectures, i.e. ZnO-passivated graphitized carbon (ZnO/C) and Pd nanoparticles on ZnO-passivated graphitized carbon (Pd/ZnO/C). The voltage profiles exhibit that the charge potential is ~4.0 V for the ZnO/C cathode, which is significantly reduced to 3.0 V for all the Pd/ZnO/C cathodes. The observed low charge potential was able to be maintained for over 10 cycles at 1000 mAh $g^{-1}$ capacity. Even more striking, a lowest charge potential at around 2.8 V is observed for the cell using the 1c-Pd/2c-ZnO/C cathode (figure 4(b)), which leads to an extremely high round-trip efficiency (>95%) of the cell. Considering that the thermodynamically determined potential of the oxygen evolution reaction from $Li_2O_2$ is 3.0 V [46, 47], such low charge potential may indicate a completely different reaction pathway from the previous literatures when the Pd/ZnO/C-based materials are used as the cathode in the Li-$O_2$ cell. While the loading of Pd affects the performance of the Li-$O_2$ battery, the effect of the ZnO loading on carbon is minor. Figures 4(c) and (e) show that the voltage profiles from the discharge/charge cycles are similar between 3c-Pd/2c-ZnO/C and 3c-Pd/5c-ZnO/C.

The above results demonstrated that the ALD Pd/ZnO tandem bilayer on carbon has been found to be effective cathode architecture for increasing the discharge capacity and for reducing the charge overpotential of Li-$O_2$ batteries. Although the mechanism is still not clear at the current stage, we do believe that both ZnO and Pd play the critical roles on enhancing the performance of the cell. In particular, the ALD ZnO thin film partially covered the carbon surface and was selectively decorated at the carbon defect sites, which help to minimize a side reaction such as electrolyte decomposition and the formation of lithium carbonate on the defect sites. Our earlier density functional theory (DFT) calculations showed that small $Al_2O_3$ islands prepared by ALD were small enough that they themselves are conductive [48]. A material that is more conductive than $Al_2O_3$, such as ZnO in this case, would be beneficial to the overall conductivity of the carbon cathode when it is used to passivate the carbon defect sites. Subsequent Pd ALD will selectively deposit uniform Pd nanoparticles on top of or at the edge of the ZnO layer because the carbon surface can be considered inert for Pd ALD. These highly dispersed Pd nanoparticles acted as the electrocatalyst for promoting the discharge and charge reactions, and consequently the electrochemical performance of the Li-$O_2$ cells is significantly improved in terms of the discharge capacity and particularly the reduction of the charge overpotential.

Finally, it should also be pointed out that the cells with a Pd/ZnO/C-based cathode started to fade with relatively short discharge/charge cycles, even under the capacity-controlled mode. Such fade is commonly observed in Li-$O_2$ cells due to the presence of the oxygen [49, 50]. As reported by Shui *et al* [51], a continuous accumulation of LiOH on the lithium anode under both charge and discharge conditions due to the oxygen-crossover effect has been observed. A large number of microscopic 'tunnels' exist within the LiOH layer, which provide a pathway for sustained ion transport by enabling the connection of lithium with the electrolyte. In this sense, the cell can be operated until the total consumption of lithium has occurred, given that the cathode and electrolyte can survive for that long period. Figure 5 showed the complete degradation of the Li anode by the corrosion of the oxygen, while the cathode still maintained its porous structure in the cells tested in this study. Compared to the Li-ion battery, the chemistry/reactions on the Li anode are far more complicated in the Li-$O_2$ battery due to the crossover effect of $O_2$, which is one of the major reasons for the degradation of the Li anode in Li-$O_2$ batteries. It is of no doubt that the protection of the Li anode against the oxygen-crossover is the key factor to improve the cycle life of the Li-$O_2$ cells.

## 4. Conclusions

In conclusion, ALD was used to deposit nanostructured palladium on ZnO-passivated porous carbon as the cathode material for Li-$O_2$ cells. Compared to the Pd/$Al_2O_3$/C cathodes [48], the ZnO-passivated ones further reduce the charge overpotential. The results demonstrated that the oxygen reduction reaction during discharge in the Li-$O_2$ cell is

significantly altered when Pd nanoparticles on ZnO-passivated carbon is used as the electrocatalyst, which not only contributes to a higher capacity by providing more active sites for the ORR reaction in the case of 3c and 10c ALD-Pd samples but also leads to a different morphology of the discharge products. The results also showed that the ALD Pd/ZnO tandem bilayer on carbon is effective cathode architecture for significantly decreasing the charge potential of Li-$O_2$ batteries, which lead to a high round-trip efficiency of the cell.

## Acknowledgments

This work was supported by the US Department of Energy under Contract DE-AC0206CH11357 from the Vehicle Technologies Office, Department of Energy, Office of Energy Efficiency and Renewable Energy (EERE). YL is grateful for the support from the UAH New Faculty Research Award. Use of the Advanced Photon Source and the Electron Microscopy Center for materials research was supported by the US Department of Energy, Office of Basic Energy Sciences, under contract no. DE-AC02-06CH11357.

## References

[1] Abraham K M and Jiang Z 1996 A polymer electrolyte-based rechargeable lithium/oxygen battery *J. Electrochem. Soc.* **143** 1–5

[2] Ogasawara T, Debart A, Holzapfel M, Novak P and Bruce P G 2006 Rechargeable $Li_2O_2$ electrode for lithium batteries *J. Am. Chem. Soc.* **128** 1390–3

[3] Jiao F and Bruce P G 2007 Mesoporous crystalline beta-$MnO_2$-a reversible positive electrode for rechargeable lithium batteries *Adv. Mater.* **19** 657–60

[4] Debart A, Paterson A J, Bao J and Bruce P G 2008 alpha-MnO (2) nanowires: a catalyst for the $O_2$ electrode in rechargeable lithium batteries *Angew. Chem., Int. Ed.* **47** 4521–4

[5] Laoire C O, Mukerjee S, Abraham K M, Plichta E J and Hendrickson M A 2009 Elucidating the mechanism of oxygen reduction for lithium-air battery applications *J. Phys. Chem.* C **113** 20127–34

[6] Williford R E and Zhang J-G 2009 Air electrode design for sustained high power operation of Li/air batteries *J. Power Sources* **194** 1164–70

[7] Andrei P, Zheng J P, Hendrickson M and Plichta E J 2010 Some possible approaches for improving the energy density of Li-air batteries *J. Electrochem. Soc.* **157** A1287–95

[8] Wang D, Xiao J, Xu W and Zhang J-G 2010 High capacity pouch-type Li-air batteries *J. Electrochem. Soc.* **157** A760–4

[9] Eswaran M, Munichandraiah N and Scanlon L G 2010 High capacity Li-O(2) cell and electrochemical impedance spectroscopy study *Electrochem. Solid-State Lett.* **13** A121–4

[10] Girishkumar G, McCloskey B, Luntz A C, Swanson S and Wilcke W 2010 Lithium—air battery: promise and challenges *J. Phys. Chem. Lett.* **1** 2193–203

[11] Hummelshøj J S, Blomqvist J, Datta S, Vegge T, Rossmeisl J, Thygesen K S, Luntz A C, Jacobsen K W and Norskov J K 2010 Communications: elementary oxygen electrode reactions in the aprotic Li-air battery *J. Chem. Phys.* **132** 071101

[12] Zhang J, Xu W, Li X and Liu W 2010 Air dehydration membranes for nonaqueous lithium-air batteries *J. Electrochem. Soc.* **157** A940–6

[13] Xiao J, Wang D, Xu W, Wang D, Williford R E, Liu J and Zhang J-G 2010 Optimization of air electrode for Li/air batteries *J. Electrochem. Soc.* **157** A487–92

[14] Lu Y-C, Gasteiger H A, Crumlin E, McGuire R Jr and Shao-Horn Y 2010 Electrocatalytic activity studies of select metal surfaces and implications in Li-air batteries *J. Electrochem. Soc.* **157** A1016–25

[15] Lu Y-C, Gasteiger H A, Parent M C, Chiloyan V and Shao-Horn Y 2010 The influence of catalysts on discharge and charge voltages of rechargeable Li-oxygen batteries *Electrochem. Solid-State Lett.* **13** A69–72

[16] Lu Y-C, Xu Z, Gasteiger H A, Chen S, Hamad-Schifferli K and Shao-Horn Y 2010 Platinum-gold nanoparticles: a highly active bifunctional electrocatalyst for rechargeable lithium-air batteries *J. Am. Chem. Soc.* **132** 12170–1

[17] Thapa A K, Saimen K and Ishihara T 2010 Pd/MnO(2) Air electrode catalyst for rechargeable lithium/air battery *Electrochem. Solid-State Lett.* **13** A165–7

[18] Bruce P G, Hardwick L J and Abraham K M 2011 Lithium-air and lithium-sulfur batteries *MRS Bull.* **36** 506–12

[19] Trahey L, Johnson C S, Vaughey J T, Kang S H, Hardwick L J, Freunberger S A, Bruce P G and Thackeray M M 2011 Activated lithium-metal-oxides as catalytic electrodes for Li-O(2) cells *Electrochem. Solid-State Lett.* **14** A64–6

[20] Wang Y and Zhou H 2011 To draw an air electrode of a Li-air battery by pencil *Energy Environ. Sci.* **4** 1704–7

[21] Xu W, Xu K, Viswanathan V V, Towne S A, Hardy J S, Xiao J, Hu D, Wang D and Zhang J-G 2011 Reaction mechanisms for the limited reversibility of Li-$O_2$ chemistry in organic carbonate electrolytes *J. Power Sources* **196** 9631–9

[22] Yoo E and Zhou H 2011 Li-air rechargeable battery based on metal-free graphene nanosheet catalysts *ACS Nano* **5** 3020–6

[23] Freunberger S A, Chen Y, Drewett N E, Hardwick L J, Barde F and Bruce P G 2011 The lithium-oxygen battery with ether-based electrolytes *Angew. Chem., Int. Ed.* **50** 8609–13

[24] Freunberger S A, Chen Y, Peng Z, Griffin J M, Hardwick L J, Barde F, Novak P and Bruce P G 2011 Reactions in the rechargeable lithium-O(2) battery with alkyl carbonate electrolytes *J. Am. Chem. Soc.* **133** 8040–7

[25] McCloskey B D, Bethune D S, Shelby R M, Girishkumar G and Luntz A C 2011 Solvents' critical rope in nonaqueous lithium-oxygen battery electrochemistry *J. Phys. Chem. Lett.* **2** 1161–6

[26] Kuboki T, Okuyama T, Ohsaki T and Takami N 2005 Lithium-air batteries using hydrophobic room temperature ionic liquid electrolyte *J. Power Sources* **146** 766–9

[27] Zhang G Q, Zheng J P, Liang R, Zhang C, Wang B, Au M, Hendrickson M and Plichta E J 2011 Alpha-$MnO_2$/carbon nanotube/carbon nanofiber composite catalytic air electrodes for rechargeable lithium-air batteries *J. Electrochem. Soc.* **158** A822–7

[28] Ren X, Zhang S S, Tran D T and Read J 2011 Oxygen reduction reaction catalyst on lithium/air battery discharge performance *J. Mater. Chem.* **21** 10118–25

[29] Lu Y-C, Gasteiger H A and Shao-Horn Y 2011 Method development to evaluate the oxygen reduction activity of high-surface-area catalysts for Li-air batteries *Electrochem. Solid-State Lett.* **14** A70–4

[30] Chung K-B, Shin J-K, Jang T-Y, Noh D-K, Tak Y and Baeck S-H 2011 Preparation and analyses of $MnO_2$/carbon composites for rechargeable lithium-air battery *Rev. Adv. Mater. Sci.* **28** 54–8

[31] Chen J, Hummelshøj J S, Thygesen K S, Myrdal J S G, Norskov J K and Vegge T 2011 The role of transition metal

interfaces on the electronic transport in lithium-air batteries *Catal. Today* **165** 2–9
[32] Lu J, Park J-B, Sun Y-K, Wu F and Amine K 2014 Aprotic and aqueous Li-$O_2$ batteries *Chem. Rev.* **114** 5611–40
[33] Puurunen R L 2005 Surface chemistry of atomic layer deposition: a case study for the trimethylaluminum/water process *J. Appl. Phys.* **97** 121301–52
[34] Leskela M and Ritala M 2002 Atomic layer deposition (ALD): from precursors to thin film structures *Thin Solid Films* **409** 138–46
[35] George S M 2010 Atomic layer deposition: an overview *Chem. Rev.* **110** 111–31
[36] Weber M J, Mackus A J M, Verheijen M A, van der Marel C and Kessels W M M 2012 Supported core/shell bimetallic nanoparticles synthesis by atomic layer deposition *Chem. Mater.* **24** 2973–7
[37] Lu J L, Low K B, Lei Y, Libera J A, Nicholls A, Stair P C and Elam J W 2014 Toward atomically precise synthesis of supported bimetallic nanoparticles using atomic layer deposition *Nat. Commun.* **5** 3264
[38] Lei Y *et al* 2012 Synthesis of Pt-Pd core–shell nanostructures by atomic layer deposition: application in propane oxidative dehydrogenation to propylene *Chem. Mater.* **24** 3525–33
[39] Elam J W, Sechrist Z A and George S M 2002 ZnO/$Al_2O_3$ nanolaminates fabricated by atomic layer deposition: growth and surface roughness measurements *Thin Solid Films* **414** 43–55
[40] Feng H, Elam J W, Libera J A, Setthapun W and Stair P C 2010 Palladium catalysts synthesized by atomic layer deposition for methanol decomposition *Chem. Mater.* **22** 3133–42
[41] Lei Y *et al* 2013 Synthesis of porous carbon supported palladium nanoparticle catalysts by atomic layer deposition: application for rechargeable lithium-$O_2$ battery *Nano Lett.* **13** 4182–9
[42] Feng H, Libera J A, Stair P C, Miller J T and Elam J W 2011 Subnanometer palladium particles synthesized by atomic layer deposition *ACS Catalysis* **1** 665–73
[43] Lu J and Stair P C 2010 Nano/subnanometer Pd nanoparticles on oxide supports synthesized by AB-type and low-temperature ABC-type atomic layer deposition: growth and morphology† *Langmuir* **26** 16486–95
[44] Shao M, Yu T, Odell J H, Jin M and Xia Y 2011 Structural dependence of oxygen reduction reaction on palladium nanocrystals *Chem. Commun.* **47** 6566–8
[45] Lu J *et al* 2014 Effect of the size-selective silver clusters on lithium peroxide morphology in lithium–oxygen batteries *Nat. Commun.* **5** 4895
[46] Bruce P G, Freunberger S A, Hardwick L J and Tarascon J-M 2012 Li-$O_2$ and Li-S batteries with high energy storage *Nat. Mater.* **11** 19–29
[47] Lu J and Amine K 2013 Recent research progress on non-aqueous lithium-air batteries from argonne national laboratory *Energies* **6** 6016–44
[48] Lu J, Lei Y, Lau K C, Luo X, Du P, Wen J, Assary R S, Das U, Miller D J and Elam J W 2013 A nanostructured cathode architecture for low charge overpotential in lithium-oxygen batteries *Nat. Commun.* **4** 2383
[49] Assary R S, Lu J, Du P, Luo X, Zhang X, Ren Y, Curtiss L A and Amine K 2013 The effect of oxygen crossover on the anode of a Li–$O_2$ battery using an ether-based solvent: insights from experimental and computational studies *ChemSusChem.* **6** 51–5
[50] Assary R S *et al* 2014 Molecular-level insights into the reactivity of siloxane-based electrolytes at a lithium-metal anode *ChemPhysChem.* **15** 2077–83
[51] Shui J L, Okasinski J S, Kenesei P, Dobbs H A, Zhao D, Almer J D and Liu D J 2013 Reversibility of anodic lithium in rechargeable lithium-oxygen batteries *Nat. Commun.* **4** 2255